Carbohydrate Polymers 236 (2020) 116023

Contents lists available at ScienceDirect

Carbohydrate Polymers

journal homepage: www.elsevier.com/locate/carbpol

The effect of dehydration/rehydration of bacterial nanocellulose on its tensile strength and physicochemical properties

Alicja Stanisławska[a], Hanna Staroszczyk[b,*], Marek Szkodo[a]

[a] Department of Mechanics Faculty of Mechanical Engineering, Poland
[b] Department of Chemistry, Technology and Biotechnology of Food, Chemical Faculty, Gdansk University of Technology, Narutowicza 11/12 St. 80-233 Gdańsk, Poland

ARTICLE INFO

Keywords:
Bacterial nanocellulose
Mechanical properties
Structural characteristics

ABSTRACT

Bacterial nanocellulose (BNC) is a natural biomaterial with a wide range of biomedical applications. BNC contains 99 % of water which makes it too thick to be used as a bioimplant material. The aim of the work was to determine the effect of the BNC dehydration followed by rehydration on its mechanical and physicochemical properties, in the context of the use of BNC as bio-prostheses in the cardiovascular system. Dehydration involved the convection-drying at 25 and 105 °C, and the freeze-drying, while rehydration - the soaking in water. All modified BNC samples had reduced thickness, and results obtained from FT-IR, XRD, and SEM analysis revealed that 25 °C BNC convection-dried after soaking in water was characterized by the highest: tensile strength (17.4 MPa), thermal stability (253 °C), dry mass content (4.34 %) and I_α/I_β ratio (1.10). Therefore, 25 °C convection-dried BNC followed by soaking in water can be considered as a material suitable for cardiovascular implants.

1. Introduction

Synthetic prostheses, made of Goretex or polypropylene, and biological protheses, made of animal materials, that are currently applied in cardiovascular surgery, are not always well tolerated by host tissues. In addition, the cost of prosthetic heart valves, vascular prostheses, and pericardial patches made of these materials is very high which, in line with a large number of vascular operations performed each year justifies the search for cheaper solutions. The implementation of bacterial nanocellulose (BNC) in the clinical practice could reduce the cost of these operations, therefore the BNC obtained on the basis of simple and cheap technologies can be an excellent alternative to previously used materials.

BNC synthesized by bacteria from *Komagataeibacter* genus is a material with unique properties including: high chemical purity as compared with plant cellulose (no lignin and hemicelluloses), high mechanical strength and absorbency, the ability to form any shape and size, inertness and non-toxicity, biocompatibility, bio-functionality and hypoallergenicity (Wang, Tavakoli, & Tang, 2019). Unfortunately, BNC obtained directly from the bacterial culture is made up of about 99 % of water and is too thick to be used as a material for the implants applied in cardiac and vascular surgery. However, an appropriate modification of BNC may initiate the creation of an alternative material for the previously used ones, with sufficient physicochemical and mechanical properties to apply it for cardiovascular implants.

There are many ways of bacterial cellulose modification. BNC can be modified chemically (modification of chemical structure and functionality) and physically (change in crystallinity, porosity, and fiber density) by applying both *in situ* and *ex situ* methods. *In situ* modifications are performed by the variation of culture media, carbon source and addition of other materials. In turn, *ex situ* modifications are realized by chemical and physical treatment of formed BNC. *In situ* modification of BNC using aloe vera (Saibuatong & Phisalaphong, 2018), chitosan (Phisalaphong & Jatupaiboon, 2008), and sodium alginate (Kanjanamosit, Muangnapoh, & Phisalaphong, 2010) has already been reported. Taisa, Stumpf, Xiuying, Jingchang and Xudong (2018) give the examples of ultrasound-assisted *in situ* modification. By *ex situ* modification, BNC composites with ZnO (Katepetch, Rujiravanit, & Tamura, 2013) and Ag (Yang, Xie, Hong, Cao, & Yang, 2012) were formed. The surface of BNC was modified by means of copolymerization reactions and cross-linking through acetylation (Kim, Nishiyam, & Kuga, 2002), phosphorylation (Hu, Chen, Yang, Li, & Wang, 2014), as well as by boiling in sodium hydroxide (McKenna, Mikkelsen, Wehr, Gidley, & Menzies, 2009).

For medical applications, such as wound dressings and patches on variable lesions, the high-water-content hydrogel biomaterial is a good choice (de Oliveira Barud et al., 2016; Picheth et al., 2017). However, sometimes, partial or complete dewatering can be important. The water

* Corresponding author.
E-mail addresses: alicja.stanislawska@pg.edu.pl (A. Stanisławska), hanna.staroszczyk@pg.edu.pl (H. Staroszczyk), marek.szkodo@pg.edu.pl (M. Szkodo).

https://doi.org/10.1016/j.carbpol.2020.116023
Received 20 September 2019; Received in revised form 14 February 2020; Accepted 14 February 2020
Available online 15 February 2020
0144-8617/

can be removed from BNC by its storage in air (intense wrinkling occurs as a result of extensive shrinkage), the use of water-absorbing materials under pressure and if necessary with additional heating (complete water removal yields films whose thickness is ca. 1% of the original thickness), stepwise solvent exchange (e.g., ethanol, acetone, hexane), drying over the gas phase (critical- point drying), and the sublimation of frozen water (freeze drying). According to Ul-Islam et al. (2013), BNC modified by dehydration through drying at different temperatures and by freeze-drying shows immense variations in structure and properties. Freeze-dried BNC has a spongy structure with pores and empty spaces, while the structure of BNC dried at 25 and 50 °C is compact and stiff.

The aim of our work was to determine the effect of the various methods of dehydration followed by the rehydration of bacterial nanocellulose on its tensile strength and physicochemical properties in the context of the potential application of BNC as a material for bio-prostheses in the human cardiovascular system. Dehydration involved the convection-drying at 25, 40, 80 and 105 °C for 48, 24, 4 and 2 h, respectively, and freeze-drying for 48 h, while rehydration involved the soaking in distilled water for 2 h. The results of preliminary studies revealed that significant differences in tensile strength values are shown by BNC convection-dried at 25 and 105 °C, and also by BNC freeze-dried; only these three BNC samples were selected for further research. All studies were carried out on BNC produced with use of a patented *Gluconacetobacter xylinus* E25 strain by the BOWIL Biotech Ltd. production facility (BOWIL Biotech Ltd. Skandynawska 7, 84-120 Władysławowo, Poland, http://www.bowil.pl). So far, nowhere in the world has bacterial BNC been produced on such a large scale. The manufacturing facility BOWIL Biotech Ltd. meets Polish and European pharmacological standards, which allows the use of BNC as a reproducible and uniform material fulfilling the norms for bioimplants. The presented research can answer the question whether the BNC subjected to dehydration/rehydration procedure can be recommended for the use as a material for cardiovascular implants.

2. Experimental procedure

2.1. Materials

2.1.1. Bacterial cultures

Bacterial nanocellulose produced by BOWIL Biotech Ltd. according to the procedure described in the PL 171952 B1 (Gałas & Krystynowicz, 1993), PL 2122003 B1 (Krystynowicz, Czaja, & Bielecki, 2003), and US 6,429,002 B1 (Ben-Bassad et al., 2002) patents was used in these experiments. Briefly, the technological process was carried out in two stages involving the pre-incubation of biomass in the submerged culture conditions and the proper surface culture of a specially selected *G. xylinus* E25 strain on a chemically well-composed and optimized medium. This medium contained a standard Herstrin-Schramm (HS) solution composed of 20 g/L glucose, 5 g/L yeast extract, 5 g/L peptone, 2.7 g/L disodium phosphate, 1.15 g/L citric acid monohydrate, 0.5 g/L magnesium sulfate, as well as 5 g/L aminobak, which is an enzymatic hydrolyzate of selected animal tissue with a high content of free amino acids and low-molecular-weight peptides. The pH of the medium and its temperature were 5.75 ± 0.03 and 30 ± 2 °C, respectively. The standard culture lasted 3 days and was carried out in a horizontal reactor with an area of 0.05 m^2 in a tray with openings to allow the flow of oxygen. There was the HS solution with addition of aminobak on the tray, which was incubated with 5–10 % (v/v) of suspension of bacterium *G. xylinus* E25. In the surface culturing, highly hydrated BNC membrane was formed after 7 days. In the next step, these membranes were purified, pressed under 345 kPa pressure and room temperature, rinsed in a tap water for 1 h, and then boiled at 80 °C in a 1% sodium hydroxide solution for 1 h and, finally in 1% acetic acid solution for another hour. After these treatments, the BNC was boiled again, first for 1 h in a tap water and then for another hour in deionized water. After each hour, the material was pressed on the press to remove excess water. Two millimeter thick material obtained this way was cut into smaller pieces and sterilized in an autoclave for 20 min at 120 °C.

2.1.2. Physical modifications of BNC

To obtain cellulosic material suitable for use in cardiac surgery, BNC containing about 98.3 % water was subjected to two types of modification. In the first case, BNC was only dried, and in the second case, after drying, BNC was additionally soaked in distilled water at 20 ± 2 °C for 2 h. Different drying methods were used in both cases. In the first method, the convection-drying at 25, 40, 80 and 105 °C for 48, 24, 4 and 2 h, respectively, and at a 35–40 % relative humidity (RH) was applied, while in the second, the freeze-drying process for 48 h, using the convection dryer with forced air circulation 130 rpm (Binder, Germany) in the first, and the Christ-Alpha 2-4 LSC in the second case (Martin Christ Gefriertrocknungsanlagen GmbH, Germany) was employed. After the BNC material had been dried, its microbiological activity was always assessed. No bacteria, yeasts or fungi were found in any of the BNC samples tested. The applied modifications allowed to obtain material of reduced thickness (300 − 500 μm), measured at five random locations with a hand-held micrometer (Brüder Mannesmann, Germany). The final thickness of BNC was similar to the thickness of natural tissues (Dawidowska & Stanisławska, 2015; Kołaczkowska et al., 2019).

2.2. Methods of testing

2.2.1. Attenuated total reflectance Fourier transformation infrared (ATR FT-IR) spectroscopy

The ATR FT-IR spectra of BNC samples were recorded in the range of 400 − 4000 cm^{-1} on a Nicolet 8700 spectrometer (Thermo Electron Scientific Inc., Waltham, MA), using a Golden Gate ATR accessory (Specac) equipped with a single-reflection diamond crystal. The temperature during measurements was kept at 25 ± 0.1 °C using an electronic temperature controller (Specac). For each spectrum, 128 scans were collected with a resolution of 4 cm^{-1}. The spectrometer's EverGlo source was on turbo mode during measurements. The spectrometer and ATR accessory were purged with dry nitrogen to diminish water-vapor contamination of the spectra. All samples were conditioned before their analysis for 7 days in a desiccator over P_2O_5. For each sample aliquot, three to five replicatespectra wererecorded to assess precision and ensurethe reproducibilityof each sample.

Second derivatives of the spectra were calculated by using the Savitzky-Golay algorithm (51 data points, ca. 25 cm^{-1}, and 3rd degree polynomial) in order to resolve the overlapping bands of individual vibrations in the region 3600–3000 cm^{-1}.

Lateral order index (LOI) (Hurtubise & Krassig, 1960; Nelson & O'Connor, 1964), total crystallinity index (TCI) (Nelson & O'Connor, 1964), and hydrogen bond intensity (HBI) (Nada, Kamel, & El-Sakhawy, 2000) calculated from the absorbance ratios A_{1429}/A_{893}, A_{1372}/A_{2892}, and A_{3336}/A_{1336} cm^{-1}, respectively, were used to study the crystallinity changes.

2.2.2. X-Ray diffractometry (XRD)

The measurements were carried out by applying CuKa radiation of wavelength of 0.154 nm in a X'Pert Pro diffractometer (Philips, Eindhoven, the Netherlands). The operation setting for the diffractometer was 30 mA and 40 kV. The spectra over the range of 5.0–50.0° 2θ were recorded at a scan rate of 0.02° 2θ /s. All BNC samples were dried in compressed air before starting the tests.

The crystallinity index (Cr.I.) of BNC was calculated based on XRD measurements by the formula given by Segal, Creely, Martin and Conrad (1959):

$$\text{Cr.I.} = [(I_{200} - I_{am})/I_{200}] \times 100$$

where I_{200} and I_{am} is the maximum intensity of diffraction at $2\theta = 22,7$ and 18°, respectively.

The crystallite size (Cr.S.) of BNC was estimated by using Scherrer formula:

$$Cr.S. = [(K \times \lambda)/(\beta \times \cos\theta)]$$

where K is a dimensionless shape factor (0.9), λ is the X-ray wavelength (0.1541 nm), β is the full width at half maximum, θ is the diffraction angle for the (200) plane (Yan, Chen, Wang, Wang, & Jiang, 2008).

2.2.3. Thermogravimetry (TGA)

Thermogravimetric analysis was performed with SDT Q600 TA (Instruments-Water LLC, New Castle, DE). The BNC samples (2 − 3 mg) were heated in open alumina crucibles in the nitrogen atmosphere, over a temperature range of 40–580 °C, at a heating rate of 10 °C /min.

2.2.4. Differential scanning calorimetry (DSC)

The BNC samples (2 − 3 mg) were sealed in aluminum pans and scanned at the rate of 10 °C/min in the temperature range of −90 to 220 °C. A TA300 DSC calorimeter (Mettler, Columbus, OH), equipped with a TC 10A processor and software ta60 version 1.31 (Shimadzu Corporation), was used with an empty pan as a reference. The instrument was calibrated against pure indium (T_m = 156.6 °C and ΔH_m = 28.45 J/g). Analyses were run in triplicates.

2.2.5. Scanning electron microscopy (SEM)

Surface morphology changes in the BNC samples were examined by means of Scanning Electron Microscopy (JSM 7800-F, Tokyo, Japan). The instrument was set for 1 kV accelerating voltage and 65 pA beam current. The instrument operated at high vacuum. The magnification range varied from 1 000–25 000 times. These measurement parameters enabled testing of non-conductive materials. To observe the cross-sections, the samples were glued with carbon tape to a carbon steel cube.

2.2.6. Mechanical tests

Tensile strength (R_m), expressed in MPa, and elongation at break (A), stated as a percentage, of the BNC samples were determined according to ASTM modified method D882-00 (ASTM, 2001), using 5543 Universal Testing Machine (Instron C., Canton, MA, USA), and they were read from the charts of stress (σ) as a function of strain (ε), σ = f (ε). Initial grip separation was 50 ± 5 mm, and cross-head speed was 10 mm/min. Prior to measurements, BNC samples that were only dried (strips whose dimensions were 15 by 100 mm) were conditioned at 25 ± 2 °C and 50 ± 2% RH for 48 h and then held in a desiccator over P_2O_5. Measurements of R_m and A for all of the other samples were carried out immediately after the removing of the samples from water.

2.2.7. Determination of dry BNC mass changes

The dry mass values for the unmodified BNC samples and samples modified by the convection-drying at 25 and 105 °C and freeze-drying were obtained after drying them for 24 h at 105 °C in a forced-air circulation oven (Binder GmbH, Germany). All samples were prepared in triplicate.

2.2.8. Statistical analysis

The results from mechanical tests are averaged from at least 14 replications. The data obtained were statistically analysed by one-way analysis of variance to determine significant differences among BNC samples, using SigmaPlot 11.0 (Softonic International S.L.). Significance was accepted at $p < 0.05$.

3. Results and discussion

3.1. BNC characterization by FT-IR spectroscopy

Table 1 lists the band assignment in the FT-IR spectrum of native BNC (Abidi, Cabrales, & Hequet, 2010; Carrilo, Colom, Suñol, & Saurina, 2004; Kacuráková, Smith, Gidley, & Wilson, 2002; Liu, Gamble, & Thibodeaux, 2010; Maréchal & Chanzy, 2000; Oh et al., 2005; Shi et al., 2014; Sugiyama, Perrson, & Chanzy, 1991). According to Halib, Amin and Ahmad (2012), FT-IR spectra of bacterial cellulose can vary slightly in terms of the position and the intensity of the bands depending on the strain applied to the culture of BNC and the measurement conditions.

The spectra of BNC dried in various conditions are presented in Fig. 1A. The changes in the FT-IR spectra of 25 °C convection-dried BNC, induced by the convection-drying process at 105 °C are demonstrated in Fig. 1B and by freeze-drying process in Fig. 1C. An analysis of the patterns of the difference bands allowed revealing the groups involved in the conformational changes caused by those processes.

The first effect which was observed because of drying was an increased absorption in the region between 3700–3100 cm^{-1} (Fig. 1A), with three positive peaks appearing at 3351, 3310, and 3240 cm^{-1} in the difference spectrum of 105 °C convection-dried BNC (Fig. 1B), and three positive peaks at 3355, 3310, and 3245 cm^{-1} in the difference spectrum of freeze-dried BNC (Fig. 1C). These peaks were due to hydrogen-bonded O—H stretching vibrations (ν_{OH}), the first intra-, and the second and third intermolecular (Table 1). Changes in the bonding of OH groups led to a shift in the maximum of the band at 3342 cm^{-1} towards higher wave numbers by 4 cm^{-1} in the spectrum of 105 °C convection-dried BNC and by 6 cm^{-1} in the spectrum of freeze-dried BNC (Fig. 1A). These shifts can be interpreted as a result of the scission of intramolecular hydrogen bonds in the cellulose structure due to drying and the release of free OH groups, which could confirm the appearance of positive peaks at 3351 and 3355 cm^{-1}, assigned to ν_{OH} (free) in the differential spectra. That OH bands region (3600 − 3000 cm^{-1}) was resolved into six individual OH bands by using the second-derivative procedure (Fig. 1D). Component peaks at 3403, 3372 and 3343 cm^{-1} were attributed to intramolecular, and those at 3296, 3271 and 3233 cm^{-1}, to intermolecular hydrogen bonds. In the

Table 1
Band assignment in the FT-IR spectra of BNC.

Position (cm^{-1}) and intensity[a]	Band assignment
3395 sh	ν_{OH} intramolecular H-bonds for 3O···H–O5 and 2O··· H–O6
3342 s	ν_{OH} intramolecular H-bonds for 3O···H–O5
3310 sh	ν_{OH} intermolecular H-bonds (corresponding to the contribution from cellulose I_β)
3240 m	ν_{OH} intermolecular H-bonds for 6O···H–O3' (corresponding to the contribution from cellulose I_α)
2893 m	ν_{CH}
1642 w	δ_{OH} polymer bound water
1428 w	δ_{OH}, δ_{CH}
1370 w	δ_{OH}, δ_{CH}
1335 w	δ_{OH}
1295 w	δ_{CH}
1162 m	$\delta_{C–O–C}$ of C1–O–C4
1105 s	$\delta_{C–OH}$ of C2–OH
1055 vs	$\delta_{C–OH}$ of C3–OH
1032 vs	$\nu_{C–O}$ of C6–OH
1003 vs	$\nu_{C–O}$
984 vs	$\nu_{C–O}$
895 w	β-glycosidic linkage
750 w	I_α, δ_{OH} out-of-plane
710 w	I_β, δ_{OH} out-of-plane

[a] Notation of the band intensity is as follows: vs – very strong, s – strong, m – medium, w – weak, sh – shoulder.

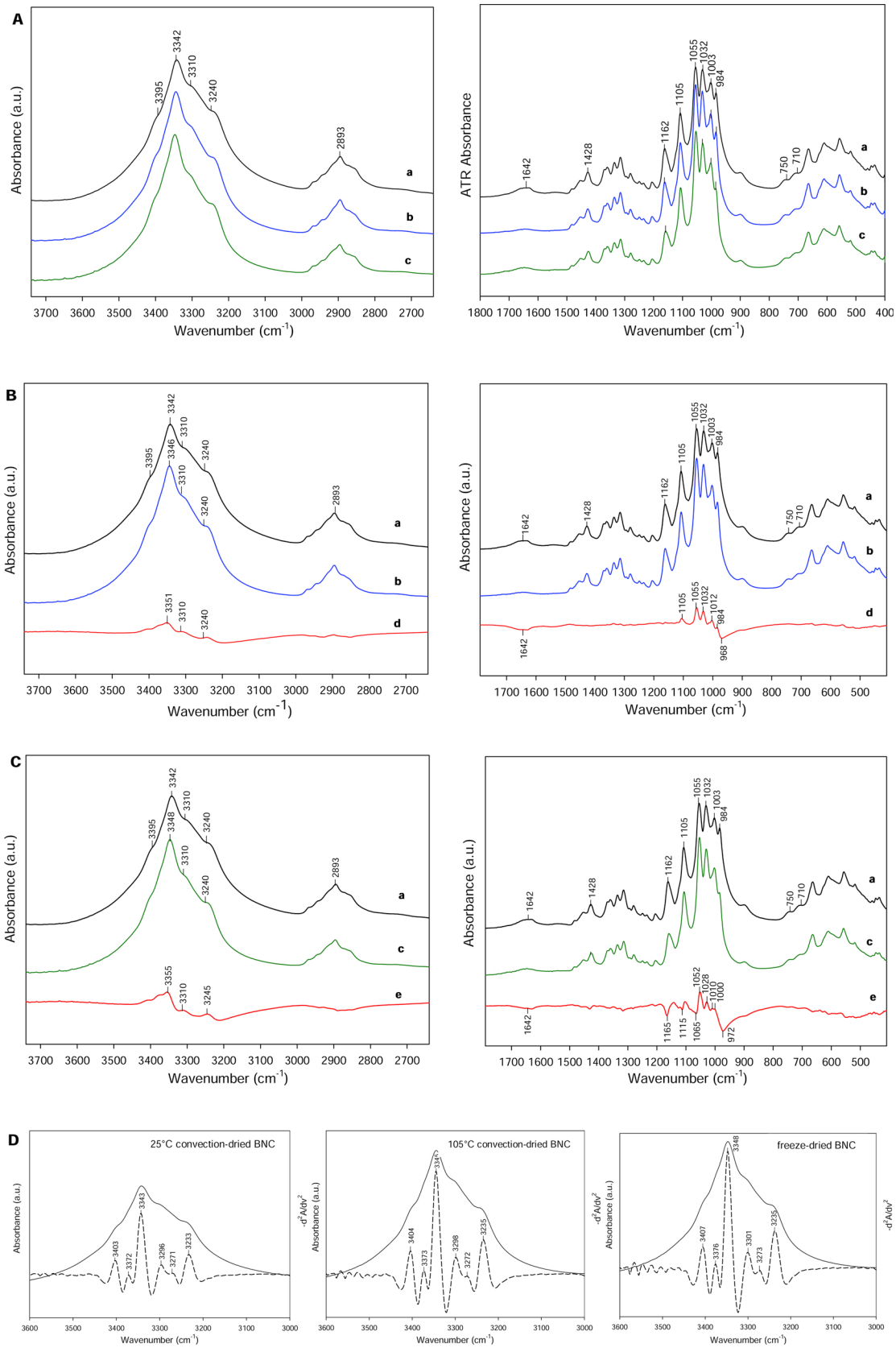

Fig. 1. FTIR spectra of (A) 25 °C convection-dried BNC (a, black line), 105 °C convection-dried BNC (b, blue line), and freeze-dried BNC (c, green line); (B) 25 °C convection-dried BNC (a, black line) and at 105 °C convection-dried BNC (b, blue line) as well as difference spectrum of the latter from which the former was subtracted (d, red line); (C) 25 °C convection-dried BNC (a, black line) and freeze-dried BNC (c, green line) as well as difference spectrum of the latter from which the former was subtracted (e, red line); (D) absorbance (solid line) and second-derivative (dotted line). (For interpretation of the references to colour in this figure legend, the reader is referred to the web version of this article).

case of spectra of 105 °C convection-dried BNC and freeze-dried BNC all these peaks were more intense and shifted by 2–5 cm^{-1} to higher wave numbers. According to Hishikawa, Togawa and Kondo (2017), and Oh et al. (2005) the band of the highest intensity at about 3343 cm^{-1} was due to intramolecular hydrogen bonds between OH group at the C-3 and C-5 position, and that at about 3222 cm^{-1}, because of intermolecular hydrogen bonds between OH group at the C-6 position and C-3′ O atom of the glucose ring of the adjacent polysaccharide chain. In turn, the band appearing at about 3403 cm^{-1} was attributed to the intramolecular hydrogen bonds between OH group at the C-2 and C-6 position of the adjacent glucose ring.

The second effect observed as a result of drying was an increased absorption in the region between 1110–1000 cm^{-1} (Fig. 1A), with positive peaks at 1105, 1055, 1032, and 1012 cm^{-1} in the corresponding spectrum of 105 °C convection-dried BNC (Fig. 1B), and at 1052, 1028, and 1010 cm^{-1} in the corresponding spectrum of freeze-dried BNC (Fig. 1C). In addition, the positive peak at 984 cm^{-1} and the negative peak at 968 cm^{-1} in the former, as well as negative peaks at 1165, 1115, 1065, 972 cm^{-1} and the positive peak at 1000 cm^{-1} in the latter difference spectrum could also be observed. These observations indicate a change in the number and in the order of the hydroxyl groups, especially those at the C2, C3, C5 and C6 of cellulose structural units and confirm that the involvement of OH groups in intra- and intermolecular hydrogen bonding changed as a result of drying. Moreover, another pattern of the difference spectrum of 105 °C convection-dried BNC compared with that of freeze-dried BNC indicates that these changes probably led to various ordered crystalline arrangements. Along with changes in the intensity of bands in the region between 3700–3100 cm^{-1} and between 1110–1000 cm^{-1}, a decrease in the intensity at 1642 cm^{-1} in the spectra of both 105 °C convection-dried BNC and freeze-dried BNC, was also noted (Fig. 1A), with the negative peak in difference spectra (Fig. 1B, C). As the intensity of that band, attributed to the OH bending mode of water (Table 1), is free from the contribution of OH groups in celluloses (Liu et al., 2010), it could be used as an index of water content in BNC. Thus, 25 °C convection-dried BNC contained more water in the structure than 105 °C convection-dried BNC and freeze-dried BNC. It is well known that a biopolymer material with a low water content usually displays lower elongation at break than that with a high water content (Vieria, da Silva, dos Santos, & Beppu, 2011), hence, it seems that the water content will affect this mechanical parameter of the tested BNC.

To estimate qualitative changes in cellulose crystallinity, HBI, LOI and TCI indexes were calculated. The data form Table 2 confirm that the number of hydrogen bonds (HBI index) in the BNC decreased due to the increase in the convection-drying temperature from 25 to 105 °C and due to the conversion from the convection-drying at 25 °C to the freeze-drying. As the HBI index decreased, the LOI and TCI indexes increased at once, which means that due to these treatments the BNC crystallinity increased. The observed trend follows previous findings (Kljun et al., 2011), and determined indexes were strongly correlated with those from XRD measurements.

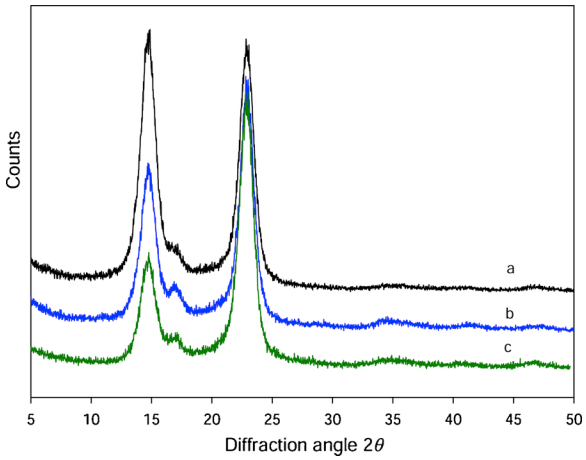

Fig. 2. XRD diffractograms of 25 °C convection-dried BNC (a, black line), 105 °C convection-dried BNC (b, blue line), and freeze-dried BNC (c, green line). (For interpretation of the references to colour in this figure legend, the reader is referred to the web version of this article).

3.2. BNC characterization by XRD analysis

Cellulose has several crystalline polymorphisms (I, II, III, IV). It is well known that bacterial cellulose secreted by *G. xylinus* is made up with cellulose I and that this type of cellulose contains two regions of higher (crystalline) and lower (amorphous) order, and exists in two different polymorphs, I_α and I_β. The I_α structure is triclinic with only one chain in a unit cell, while the I_β structure is monoclinic with two chains per unit cell. Bacterial cellulose was reported to possess a considerable amount of the I_α allomorph with the I_α/I_β = 65/35 (Kondo, Rytczak, & Bielecki, 2016). According to Sugiyama et al. (1991) the I_α form of cellulose is metastable and can be readily and easily converted to the stable I_β form by hydrothermal treatment. However, complete conversion to I_β is typically not achieved (Moon, Martini, Nairn, Siomonsen, & Youngblood, 2011).

XRD diffraction patterns of the BNC dried under different conditions are shown in Fig. 2. All of those patterns are characterized by two sharp intense peaks at 14.7 and 22.7° 2θ, and by the peak at 16.8° 2θ of the lower intensity. They correspond to the primary diffraction of the crystal plane ($1\bar{1}0$), (200) and (110), respectively, which points to the structure of a well-defined cellulose I crystal (Shi et al., 2014). Additionally, the peak at 14.7° is characteristic of cellulose I_α and that at 22.7° 2θ of cellulose Iβ (Vasquez, Foresti, Cerrutti, & Galvagno, 2013).

When comparing the I_α/I_β ratio (Table 2), calculated by dividing the area under the peak at 22.7° by the area under the peak at 14.7°, it is clear that the proportion of cellulose I_α in the 25 °C convection-dried BNC is higher than cellulose I_β, but decreased as a result of change in the drying conditions. Thus, the change in intra- and intermolecular hydrogen bonding in the BNC structure due to its drying affected the ratio between both polymorphisms. However, despite significant changes in the diffraction patterns, no changes in the intensity of

Table 2
Effect of drying method on the crystallinity changes in BNC.

Drying method	Cr.S. (nm)	Cr.I. (%)	I_α/I_β [a,b]	LOI[b]	HBI[b]	TCI[b]
Convection-drying at 25 °C	5,70	90.6	1.10 ± 0.19	1.02 ± 0.20	5.20 ± 1.00	0.49 ± 0.09
105 °C	7,70	90.8	0.72 ± 0.08	1.30 ± 0.14	4.37 ± 0.48	0.70 ± 0.08
Freeze-drying	7,98	91.6	0.48 ± 0.05	1.57 ± 0.16	4.52 ± 0.45	0.79 ± 0.08

[a] I_α/I_β was calculated by dividing the area of peak at 22.7° by the area of peak at 14.7° visible on the diffraction patterns shown in Fig. 4. The areas were calculated using Origin software.
[b] Mean value of 3 measurements ± standard deviation.

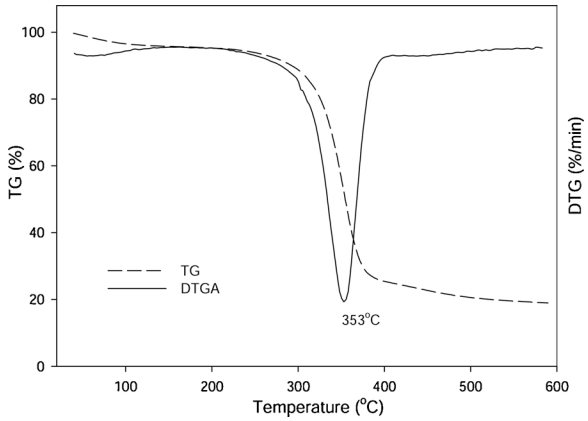

Fig. 3. TGA thermogram of 25 °C convection-dried BNC.

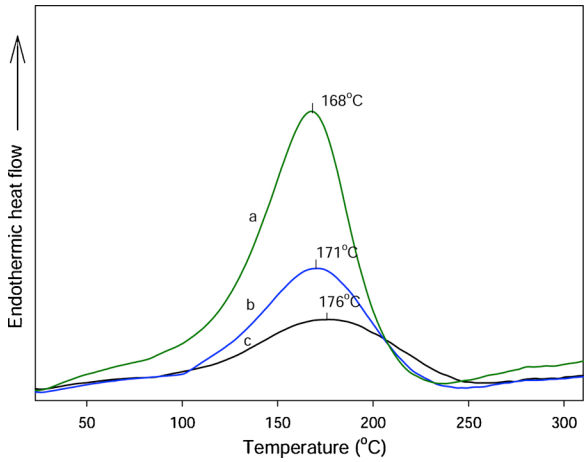

Fig. 4. DSC thermograms of 25 °C convection-dried BNC (a, black line), 105 °C convection-dried BNC (b, blue line), and freeze-died BNC (c, green line). (For interpretation of the references to colour in this figure legend, the reader is referred to the web version of this article).

absorption bands at 3270 and 710 cm^{-1}, attributed to cellulose I_β phase, and those at 3250 and 750 cm^{-1}, assigned to cellulose I_α phase (Table 1) were observed in the FT-IR spectra of BNC dried under different conditions. Such changes were observed by Sugiyama et al. (1991) who analyzed the structural changes in the cellulose of different origin during heat treatment.

The crystallinity index Cr.I. of 25 °C convection-dried BNC was 90.6 % (Table 2). After increasing the drying temperature from 25 to 105 °C and after the conversion of the convection-drying to the freeze-drying, Cr.I., and also Cr.S., slightly increased. These findings confirm the results obtained from the analysis of FT-IR spectra.

3.3. BNC thermal characterization by TGA and DSC analysis

The TGA thermogram presented in Fig. 3 demonstrates that the total weight loss of 25 °C convection-dried BNC occurred at 253 °C, and at 580 °C it was 80.92 % (Table 3). There were no distinct differences in the shapes of thermograms of BNC dried under different conditions, and insight in the pattern of the TG lines (Table 3) revealed that all BNC samples were non-hygroscopic, as up to 96 °C all of them lost about 5–7 % of adsorbed water. Moreover, 105 °C convection-dried BNC and freeze-dried BNC were thermally slightly less stable, as they decomposed faster, i.e. at temperatures lower by 2 and 8 °C, respectively, lower, than 25 °C convection-dried BNC.

The lower thermal stability of 105 °C convection-dried BNC and freeze-dried BNC as compared to 25 °C convection-dried BNC was also revealed by DSC thermograms (Fig. 4). Both of those DSC thermograms, especially that of freeze-dried BNC, indicated also a higher ordered structure than the structure of 25 °C convection-dried BNC, showed by narrower melting peaks.

The decrease in the thermal stability with the increase of structure order indicated by TGA and DSC thermograms correlated well with LOI and TCI indexes calculated on the basis of FTIR spectra as well as with the Cr.I. calculated on the basis of XRD diffraction patterns (Table 2).

Table 3
Thermogravimetric characteristics of BNC subjected to the drying process.

Temperature range (°C)	Drying method					
	Convection-drying at 25 °C		Convection-drying at 105 °C		Freeze-drying	
	Weight loss (%)[a]	DTG (°C)	Weight loss (%)[a]	DTG (°C)	Weight loss (%)[a]	DTG (°C)
40-200	4.74		5.91		7.27	
200-400	69.82	253	68.80	251	66.92	245
400-580	6.36		5.94		5.85	
Total	80.92		80.65		80.04	

[a] Percentage of weight loss during the special temperature ranges.

3.4. BNC characterization by SEM analysis

During the synthesis process, BNC fibers aggregate and are immobilized in a stable, well-defined cellulose network due to the presence of hydrogen bonds and van der Waals forces. According to Gama, Gatenholm and Klemm (2017) these forces cause filaments to interact with each other and to be kept separately by adsorbed water layers. The hydrophilicity of BNC membranes is usually explained by the presence of the structure of pores and tunnels (Klemm, Schummann, Udhardt, & Marsch, 2001). Thus, water plays a key role as a spacer and as a stabilizing factor for the network and pore structure due to the interaction of hydrogen bonds with cellulose.

BNC dried at different conditions had a similar surface and exhibited a typical structure for cellulose (Fig. 5A). The SEM images of convection-dried or freeze-dried BNC taken at 1000x magnification revealed either the shrinkage or the smooth surface, respectively. The strongest wrinkled surface was visible for 25 °C convection-dried BNC. A higher degree of corrugation of the surface of convection-dried BNC than freeze-dried BNC may indicate that higher compressive stresses are generated during convection drying. The compressive stresses created after drying process, can cause an increase in the tensile strength, because the forces applied to the material must first overcome them and only then they contribute to the stretching of cellulose fibers. As the SEM images showed, 25 °C convection-dried BNC had the most corrugated surface. That BNC was also characterized by the highest resistance to tensile.

In the SEM images taken at 25 000x magnification, numerous pores formed from intersecting fibers were observed (Fig. 5A). The diameter of the pores in 25 °C convection-dried BNC was the smallest and it was about 80 nm, while the pores present in 105 °C convection-dried BNC and freeze-dried BNC had similar diameters amounting to ca. 100 nm. According to Ul-Islam et al. (2013), larger pores and lower density of freeze-dried BNC than that of convection-dried BNC contribute to easier water penetration of the former, and consequently, to the reduction in its tensile strength. The tensile strength of BNC soaked after previous freeze-drying and convection-drying at 105 °C was 2 times lower than that of non-soaked BNC (Table 4). Hence, it seems that freeze-dried BNC and 105 °C convection-dried BNC have similar ease of water penetration. These two BNC samples also showed an undulating surface, which can indicate a lack of residual stress or occurrence of tensile stress also facilitating water penetration. The BNC convection-dried at

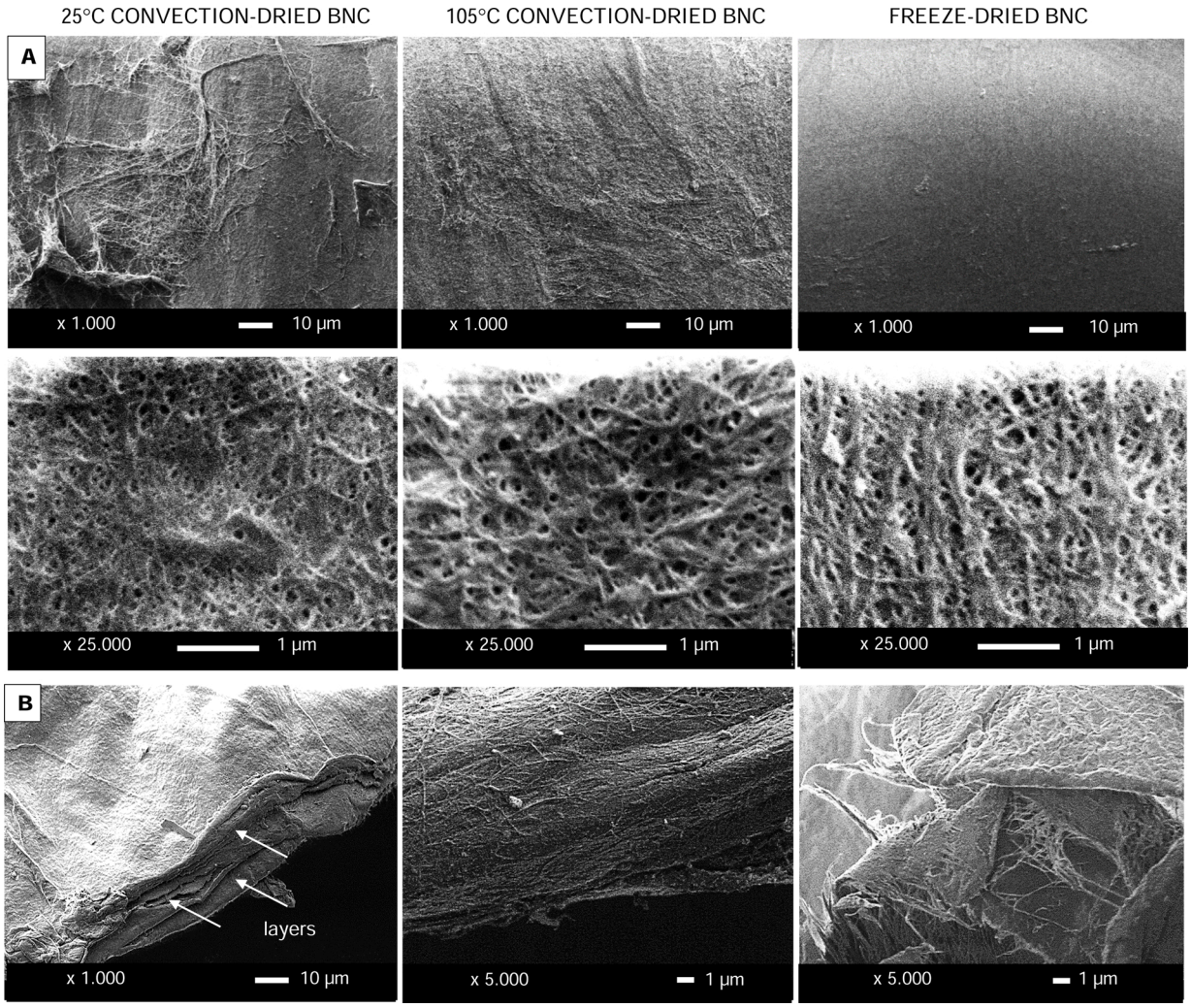

Fig. 5. Scanning electron micrographs of BNC dried under different conditions: surface (A), cross-section (B).

Table 4
Effect of drying method and temperature on mechanical properties of BNC.

BNC	R_m (MPa)[n]	A (%)[n]	Dry mass (%)[m]
Non-dried	1.18 ± 1.01[f]	12.80 ± 2.17[a]	1,76 ± 0.32[a]
Convection-dried at 25 °C	17.38 ± 7.23[a,b]	6.63 ± 1.55[b,c,d]	4.34 ± 0.82[e]
then soaked	17.40 ± 3.68[a,b]	11.04 ± 3.68[a,b]	
40 °C	17.28 ± 4.64[a,b]	6.18 ± 0.92[d]	3.57 ± 0.53[d,e]
then soaked	16.98 ± 4.34[a,b]	8.87 ± 1.73[a,b,c]	
80 °C	12.94 ± 1.80[b,c,]	6.40 ± 1.61[b,c,d]	3.44 ± 0.37[d,e]
then soaked	8.49 ± 5.47[b,c,d]	11.08 ± 2.75[a,b]	
105 °C	12.56 ± 2.45[b,c]	6.54 ± 2.57[a,b,c,d]	3.68 ± 0.40[d,e]
then soaked	5.23 ± 1.59[e]	12.85 ± 4.18[a]	
Freeze-dried	21.67 ± 6.02[a]	3.04 ± 0.85[e]	3.36 ± 0.34[b,c,d]
then soaked	10.04 ± 2.32[b,c,d]	8.25 ± 0.84[a,b]	

[n] and [m] Mean value of 14 and 3 measurements, respectively, ± standard deviation; the values in the columns marked with various letters differ significantly ($p < 0.05$).

25 °C is characterized by wrinkled surface, which suggests the occurrence of compressive stress impeding the penetration of water. BNC dried in this way did not decrease its tensile strength after soaking. Microscopic examination also allowed the identification of the mechanism of BNC fracture under the influence of stretching stresses. The applied loads cause the breaking of individual fibers or their weave composed of a small number of fibers which leads to the formation of pores which, in turn, reduce the cross-section of the transferred loads. Successively, this leads to increased stresses and the formation of subsequent pores, which reduce the stress even further, until the material ruptures. As the smaller pores after the tensile test occurred in the BNC dried at lower temperatures (Fig. 5B), it can be concluded that drying at lower temperatures leads to thicker cellulose fiber strands or increased strength of individual fibers contributing to the delay of pore formation in the tensile test. The cross section of the 25 °C convection-dried BNC shows layered structure of the material (Fig. 5B). Separation of individual layers can also be observed. The individual layers are torn, which leads to a reduction in the load-carrying cross section up to the final tear of the material. For BNC samples subjected to convection-drying at 25 °C and 105 °C, cross-sections are fragile. In the case of freeze-dried BNC, cross-section toughness can be observed. For this sample, after the tensile test, BNC fibers are pulled and torn.

3.5. Mechanical properties of BNC

Mechanical properties of BNC depend on many factors, including bacterial strain used for its production, the composition of culture medium, the method of BNC purification from the culture liquid and the method of the BNC drying (Hsieh, Yano, & Eichhorn, 2008; Saska et al., 2012; Ul-Islam, Khan, & Park, 2012; Yano, Maeda, Nakajima, Hagiwara, & Sawaguchi, 2008; Zhijiang & Guang, 2011). The effects of the latter factor on the R_m and the A of BNC are shown in Table 4.

Both convection-drying and freeze-drying increased mechanical

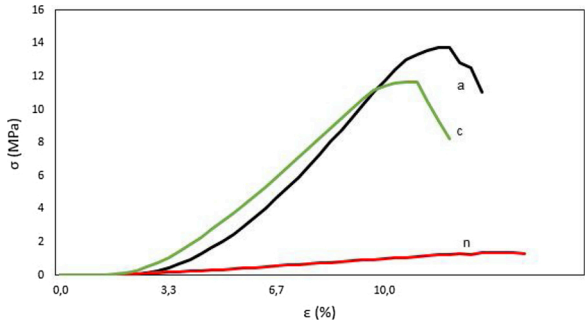

Fig. 6. Tensile test graphs of 25 °C convection-dried BNC (a, black line), freeze-dried BNC (c, green line), and native BNC (n, red line). (For interpretation of the references to colour in this figure legend, the reader is referred to the web version of this article).

strength and decreased elongation at break of native (non-dried) BNC. The R_m value of freeze-dried BNC was ca. 18 times higher than that of non-dried BNC, while the R_m of 25 °C convection-dried BNC was ca. 15 times higher than this value, and was decreasing with the increase of the drying temperature to 105 °C. The A value of all dried samples was low, regardless of the drying method, however, the A of freeze-dried BNC was about two times lower than that of convection-dried BNC at both temperatures applied. Thus, the results of mechanical tests confirm the previous suppositions, that the water contained in the BNC structure will affect its mechanical parameters. BNC samples with the highest water content, which was first estimated from FT-IR spectra (Fig. 1), and then from the TGA analysis (Table 3), and with the lowest dry mass content (Table 4) showed the highest R_m values and the lowest A values. In turn, those with the lowest water content and the highest dry mass content, conversely, showed the lowest R_m and the highest A.

The soaking of previously dried BNC resulted in a decrease in R_m and an increase in A, irrespective of the drying method; however, R_m of any soaked BNC sample did not decrease to the R_m value of non-dried BNC. The higher decrease in the R_m as a result of soaking occurred in the 105 °C convection-dried BNC, and the smaller in 25 °C convection-dried BNC. The A value of convection- and freeze-dried BNC after soaking was almost two and three times higher, respectively, than that of non-soaked BNC.

Two typical stress-strain curves recorded for non-dried BNC and that subjected to convection-drying at 25 °C with subsequent soaking in distilled water are shown in Fig. 6. This figure revealed a partial strengthening of the BNC occurring immediately prior to its breaking, both for non-dried and dried samples that were soaked. The strengthening manifests itself in the $\sigma = f(\varepsilon)$ graph with a characteristic decrease, followed by an increase in the stresses immediately prior to the final sample breaking. Strengthening could be caused by the ordering of cellulosic fibers in the direction of stretching, i.e. increase in the degree of crystallinity of the material. The chart shows that in native BNC such a strengthening can be seen, as opposed to the modified BNC (dried in 25 °C and then soaked and freeze-dried and then soaked). The probable cause of this phenomenon is that the native material has a lower degree of fibre arrangement than the material after modification. Modified material is already strengthened and the tensile test does not further strengthen the material. It may be likely that the lower tensile strength is accompanied by the greater strengthening during the tensile test.

It can be concluded that 25 °C convection-dried BNC soaked in distilled water, with R_m and A values of 17.4 MPa and 11 %, respectively, had optima strength properties allowing the use such cellulosic material as a biological implant of the circulatory system. The R_m value of such modified BNC was about 15 times higher than that of BNC not subjected to drying, with only a slightly lower value of A compared to A measured for non-dried BNC. Moreover, the R_m of 25 °C convection-dried BNC was at least three times higher than the R_m of natural porcine circulatory tissues as determined in the authors' previous research (Dawidowska & Stanisławska, 2015; Kołaczkowska et al., 2019). That research showed that the R_m of left coronary petal, right coronary petal, coronaryless petal, and lobe of aorta were in the range 2.25–3.05 MPa, 3.93–4,27 MPa, 2.78-1.92 MPa, and 1.50–1.75 MPa, respectively.

4. Conclusions

BNC dehydrated by convection-drying at 25 °C and then hydrated by soaking in distilled water for 2 h yields a final product with the reduced thickness, similar to that of natural tissues, and with improved mechanical properties, i.e. with tensile strength of 17.4 MPa and elongation at break of 11.04 %. These properties result from the modified structure of BNC. BNC convection-dried at 25 °C is characterized by the lower water content and the higher dry mass content than that convection-dried at 105 °C and that freeze-dried, and by the higher number of hydrogen bonds in its structure. These features affect the higher I_α/I_β ratio and the higher thermal stability of BNC convection-dried at 25 °C than at 105 °C and then BNC freeze dried. Therefore, from among all studied samples, 25 °C convection-dried BNC followed by its soaking in water is the material which can be recommended for further research to examine if it fulfils the requirements for artificial heart valves.

Autors' contributions

Alicja Stanisławska carried out all experiments and was involved in the editing of manuscript.

Marek Szkodo was involved in discussion on the experimental findings and in the editing of manuscript.

Hanna Staroszczyk prepared the final version of manuscript.

Acknowledgments

This work was supported by the Polish national research budget, under the National Centre Research and Development grant number PBS2/A7/16/2013.

References

Abidi, N., Cabrales, L., & Hequet, E. (2010). Fourier transform infrared spectroscopic approach to the study of the secondary cell wall development in cotton fiber. *Cellulose, 17*, 309–320. https://doi.org/10.1007/s10570-009-9366-1.

ASTM (2001). *Standard test method for tensile properties of thin plastic sheeting. D 882-00. Annual book of ASTM 2001.* Philadelphia, PA: American Society for Testing and Materials.

Ben-Bassad, A., Burner, R., Shoemaker, S., Aloni, Y., Wong, H., Johnson, D. C., et al. (2002). *Reticulated cellulose producing Acetobacter strains.* US 6,426,002 B.

Carrilo, F., Colom, X., Suñol, J. J., & Saurina, J. (2004). Structural FTIR analysis and thermal characterization of lyocell and viscose-type fibres. *European Polymer Journal, 40*, 2229–2234. https://doi.org/10.1016/j.eurpolymj.2004.05.003.

Dawidowska, K., & Stanisławska, A. (2015). Influence of preservative on the tensile strength of the tissue of porcine circulatory system. *Advanced Materials Science, 15*, 67–75. https://doi.org/10.1515/adms-2015-0017.

de Oliveira Barud, H. G., da Silva, R. R., da Silva Barud, H., Tercjak, A., Gutierrez, J., Lustri, W. R., et al. (2016). A multipurpose natural and renewable polymer in medical applications: Bacterial cellulose. *Carbohydrate Polymers, 153*, 406–420. https://doi.org/10.1016/j.carbpol.2016.07.059.

Gałas, E., & Krystynowicz, A. (1993). *Sposób wytwarzania celulozy bakteryjnej.* PL 171952 B1.

Gama, M., Gatenholm, P., & Klemm, D. (2017). *Bacterial nanocellulose: A sophisticated multifunctional material.* Boca Raton, London, New York: CRC Press.

Halib, N., Amin, M. C. I. M., & Ahmad, I. (2012). Physicochemical properties and characterization of nata de coco from local food industries as a source of cellulose. *Sains Malaysiana, 41*, 205–211.

Hishikawa, Y., Togawa, E., & Kondo, T. (2017). Characterization of individual hydrogen bonds in crystalline regenerated cellulose using resolved polarized FTIR spectra. *ACS Omega, 2*, 1469–1476. https://doi.org/10.1021/acsomega.6b00364.

Hsieh, Y. C., Yano, H. N. M., & Eichhorn, S. J. (2008). An estimation of the Young's modulus of bacterial cellulose filaments. *Cellulose, 15*, 507–513. https://doi.org/10.1007/s10570-008-9206-8.

Hu, W., Chen, S., Yang, J., Li, Z., & Wang, H. (2014). Functionalized bacterial cellulose derivatives and nanocomposites. *Carbohydrate Polymers, 101*, 1043–1060. https://doi.org/10.1016/j.carbpol.2013.09.102.

Hurtubise, F., & Krassig, H. (1960). Classification of fine structural characteristics in

cellulose by infrared spectroscopy. *Analytical Chemistry, 32*, 177–181. https://doi.org/10.1021/ac60158a010.
Kacuráková, M., Smith, A. C., Gidley, M. J., & Wilson, R. H. (2002). Molecular interactions in bacterial cellulose composites studied by 1D FT-IR and dynamic 2D FT-IR spectroscopy. *Carbohydrate Research, 337*, 1145–1153. https://doi.org/10.1016/S0008-6215(02)00102-7.
Kanjanamosit, N., Muangnapoh, C., & Phisalaphong, M. (2010). Biosynthesis and characterization of bacteria cellulose–alginate film. *Journal of Applied Polymer Sciences, 115*, 1581–1588. https://doi.org/10.1002/app.31138.
Katepetch, C., Rujiravanit, R., & Tamura, H. (2013). Formation of nanocrystalline ZnO particles into bacterial cellulose pellicle by ultrasonic-assisted in situ synthesis. *Cellulose, 20*, 1275–1292. https://doi.org/10.1007/s10570-013-9892-8.
Kim, D. Y., Nishiyam, Y., & Kuga, S. (2002). Surface acetylation of bacterial cellulose. *Cellulose, 9*, 361–367. https://doi.org/10.1023/A:1021140726936.
Klemm, D., Schummann, D., Udhardt, U., & Marsch, S. (2001). Bacterial synthesized cellulose – Artificial blood vessels for microsurgery. *Progress in Polymer Science, 26*, 1561–16003. https://doi.org/10.1016/S0079-6700(01)00021-1.
Kljun, A., Benians, T. A. S., Goubet, F., Meulewaeter, F., Knox, J. P., & Blackburn, R. S. (2011). Comparative analysis of crystallinity changes in cellulose I polymers using ATR-FTIR, X-ray diffraction, and carbohydrate-binding module probes. *Biomacromolecules, 12*, 4121–4126. https://doi.org/10.1021/bm201176m.
Kołaczkowska, M., Siondalski, P., Kowalik, M. M., Pęksa, R., Długa, A., Zając, W., et al. (2019). Assessment of the usefulness of bacterial cellulose produced by Gluconacetobacter xylinus E25 as a new biological implant. *Materials Science & Engineering C: Materials for Biological Applications, 97*, 302–312. https://doi.org/10.1016/j.msec.2018.12.016.
Kondo, T., Rytczak, P., & Bielecki, S. (2016). Bacterial nanocellulose characterization. In F. Gama, F. Dourado, & S. Bielecki (Eds.). *Bacterial nanocellulose. From biotechnology to bio-economy* (pp. 59–71). Amsterdam, Netherlands: Elsevier.
Krystynowicz, A., Czaja, W., & Bielecki, S. (2003). *Sposób otrzymywania celulozy bakteryjnej.* PL 212003 B1.
Liu, Y., Gamble, G., & Thibodeaux, D. (2010). Development of Fourier transform infrared spectroscopy in direct, non-destructive, and rapid determination of cotton fiber maturity. *Applied Spectroscopy, 64*, 1355–1363. https://doi.org/10.1177/0040517511410107.
Maréchal, Y., & Chanzy, H. (2000). The hydrogen bond network in I_β cellulose as observed by infrared spectrometry. *Journal of Molecular Structure, 523*, 183–196. https://doi.org/10.1016/S0022-2860(99)00389-0.
McKenna, B. A., Mikkelsen, D., Wehr, J. B., Gidley, M. J., & Menzies, N. W. (2009). Mechanical and structural properties of native and alkali-treated bacterial cellulose produced by Gluconacetobacter xylinus strain ATCC 53524. *Cellulose, 16*, 1047–1055. https://doi.org/10.1007/s13197-011-0401-5.
Moon, R. J., Martini, A., Nairn, J., Siomonsen, J., & Youngblood, J. (2011). Cellulose nanomaterials review: Structure, properties and nanocomposites. *Chemical Society Reviews, 40*, 3941–3994. https://doi.org/10.1039/C0CS00108B.
Nada, A.-A. M. A., Kamel, S., & El-Sakhawy, M. (2000). Thermal behaviour and infrared spectroscopy of cellulose carbamates. *Polymer Degradation and Stability, 70*, 347–355. https://doi.org/10.1016/S0141-3910(00)00119-1.
Nelson, M. L., & O'Connor, R. T. (1964). Relation of certain infrared bands to cellulose crystallinity and crystal lattice type. Part I. Spectra of lattices types I, II, III, and of amorphous cellulose. *Journal of Applied Polymer Science, 8*, 1311–1324. https://doi.org/10.1002/app.1964.070080322.
Oh, S. Y., Yoo, D. I., Shin, Y., Kim, H. C., Kim, H. Y., Chung, Y. S., et al. (2005). Crystalline structure analysis of cellulose treated with sodium hydroxide and carbon dioxide by means of X-ray diffraction and FTIR spectroscopy. *Carbohydrate Polymers, 340*, 2376–2391. https://doi.org/10.1016/j.carres.2005.08.007.
Phisalaphong, M., & Jatupaiboon, N. (2008). Biosynthesis and characterization of bacteria cellulose–chitosan film. *Carbohydrates Polymers, 74*, 482–488. https://doi.org/10.1016/j.carbpol.2008.04.004.
Picheth, G. F., Pirich, C. L., Sierakowski, M. R., Woehl, M. A., Sakakibara, C. N., de Souza, C. F., et al. (2017). Bacterial cellulose in biomedical applications: A review. *International Journal of Biological Macromolecules, 104*(Pt A), 97–106. https://doi.org/10.1016/j.ijbiomac.2017.05.171.
Saibuatong, O. A., & Phisalaphong, M. (2018). Novo aloe vera–bacterial cellulose composite film from biosynthesis. *Carbohydrates Polymers, 79*, 455–460. https://doi.org/10.1016/j.carbpol.2009.08.039.
Saska, S., Teixeira, L. N., de Oliveir, P. T., Gaspar, A. M. M., Ribeiro, S. J. L., Messaddeq, Y., et al. (2012). Bacterial cellulose-collagen nanocomposite for bone tissue engineering. *Journal of Material Chemistry, 22*, 22102–22112. https://doi.org/10.1039/C2JM33762B.
Segal, L., Creely, J. J., Martin, A., & Conrad, C. M. (1959). An empirical method for estimating the degree of crystallinity of native cellulose using the X-ray diffractometer. *Textile Research Journal, 29*, 786–794. https://doi.org/10.1177/004051755902901003.
Shi, X., Cui, Q., Zheng, Y., Peng, S., Wang, G., & Xie, Y. (2014). Effect of selective oxidation of bacterial cellulose on degradability in phosphate buffer solution and their affinity for epidermal cell attachment. *RSC Advanced, 4*, 60749–60756. https://doi.org/10.1039/C4RA10226F.
Sugiyama, Perrson, J., & Chanzy, H. (1991). Combiner infrared and electron diffraction study of the polymorphism of native celluloses. *Macromolecules, 24*, 2461–2466. https://doi.org/10.1021/ma00009a050.
Taisa, R., Stumpf, Xiuying, Y., Jingchang, Z., & Xudong, C. (2018). In situ and ex situ modifications of bacterial cellulose for applications in tissue engineering. *Materials Science and Engineering C, 82*, 372–383. https://doi.org/10.1016/j.msec.2016.11.121.
Ul-Islam, M., Khan, T., & Park, J. K. (2012). Nanoreinforced bacterial cellulose–montmorillonite composites for biomedical applications. *Carbohydrate Polymers, 89*, 1189–1197. https://doi.org/10.1016/j.carbpol.2012.03.093.
Ul-Islam, M., Khattak, W. A., Kang, M., Kim, S. M., Khan, T., & Pakr, J. K. (2013). Effect of post-synthetic processing conditions on structural variations and applications of bacterial cellulose. *Cellulose, 20*, 253–263. https://doi.org/10.1007/s10570-012-9799-9.
Vasquez, A., Foresti, M. L., Cerrutti, P., & Galvagno, M. (2013). Bacterial cellulose from simple and low cost production media by *Gluconacetobacter xylinus*. *Journal of Polymers and the Environment, 21*, 545–554. https://doi.org/10.1007/s10924-012-0541-3.
Vieria, M. G. A., da Silva, M. A., dos Santos, L. O., & Beppu, M. M. (2011). Natural-based plasticizers and biopolymer films: A review. *European Polymer Journal, 47*, 254–263. https://doi.org/10.1016/j.europolymj.2010.12.011.
Wang, J., Tavakoli, J., & Tang, T. (2019). Bacterial cellulose production, properties and applications with different culture methods – A review. *Carbohydrate Polymers, 219*, 63–76. https://doi.org/10.1016/j.carbpol.2019.05.008.
Yan, Z., Chen, S., Wang, H., Wang, B., & Jiang, J. (2008). Biosynthesis of bacterial cellulose/multi-walled carbon nanotubes in agitated culture. *Carbohydrate Polymers, 74*, 659–665. https://doi.org/10.1016/j.carbpol.2008.04.028.
Yang, G., Xie, J. J., Hong, F., Cao, Z. J., & Yang, X. X. (2012). Antimicrobial activity of silver nanoparticle impregnated bacterial cellulose membrane: Effect of fermentation carbon sources of bacterial cellulose. *Carbohydrate Polymers, 87*, 839–845. https://doi.org/10.1016/j.carbpol.2011.08.079.
Yano, S., Maeda, H., Nakajima, M., Hagiwara, T., & Sawaguchi, T. (2008). Preparation and mechanical properties of bacterial cellulose nanocomposites loaded with silica nanoparticles. *Cellulose, 15*, 111–120. https://doi.org/10.1007/s10570-007-9152-x.
Zhijiang, C., & Guang, Y. (2011). Bacterial cellulose/collagen composite: Characterization and first evaluation of cytocompatibility. *Journal of Applied Polymer Science, 120*, 2938–2944. https://doi.org/10.1002/app.33318.